Cross section reconstruction during uniaxial loading

M R Arthington, C R Siviour, N Petrinic and B C F Elliott

Department of Engineering Science, University of Oxford, Parks Road, OX1 3PJ, UK

E-mail: matthew.arthington@eng.ox.ac.uk, clive.siviour@eng.ox.ac.uk, nik.petrinic@eng.ox.ac.uk, ben.elliott@eng.ox.ac.uk

Abstract.

The inelastic response of materials to applied uniaxial loading is typically measured using tensile or compressive specimens of initially circular cross-section. Under deformation, this cross-section may become elliptical due to anisotropic material behaviour.

An optical technique for measuring the elliptical deformation of anisotropic, homogeneous cylindrical specimens undergoing uniaxial deformation is presented. It enables the quantification of anisotropic deformation in-situ and provides data for material characterisation.

Three or more silhouette views of a specimen are obtained using multiple cameras or mirrored views. The positions of the edges are computed using a sub-pixel edge detection method and 3D tangent rays from the camera through these positions are calculated. These bounding tangents are used as the basis for an elliptical fit by least squares at cross sections along the length of the specimen.

Stochastic error estimates are performed by simulation of the experiment. Error estimates, for the experimental set-up used, are also calculated by reconstructing elliptical prisms of precisely measured dimensions. Example reconstructions from specimens of rolled titanium deformed plastically in tension at quasi-static (7×10^{-4} s^{-1}) and high strain rates (3×10^{3} s^{-1}) are presented.

Keywords: 3D reconstruction, image processing, ellipse, material behaviour, anisotropic, split-Hopkinson Bar

1. Introduction

The use of any material in real life structural applications requires a knowledge of its mechanical properties, in particular its response to applied loading at different strain rates and temperatures [1]. A common technique for measuring these properties is the uniaxial tensile test on cylindrical dog-bone specimens. Calculation of true stress in these specimens requires knowledge of the cross-section as a function of time.

Complications arise when the material being tested does not deform axisymmetrically - the cross-section is no longer a circle - as a result of anisotropy. In order to determine the parameters that govern plastic anisotropy in metals, it has been shown [2] that the ratio of the strains perpendicular to the uniaxial loading direction may be used, which may be determined from the shape of the cross-section.

Optical methods offer the best means of measuring these cross-sections, since multi-point measurements can be made, they operate at all strain rates for which photographs can be taken, without significant alteration to the post processing and can be applied to environmentally controlled experiments. Optical techniques for measuring two dimensional geometry from a single view of specimens are commonplace, e.g. [3], however a means of constructing the 3D specimen shape from 2D images is required for anisotropic deformation of specimens.

In this paper, a method is proposed and evaluated for the reconstruction of the cross-section in 3D of anisotropic, homogeneous specimens undergoing uniaxial loading at any strain rate. An optical contour reconstruction method is used which reduces the cross-sectional shape fitting problem to one of fitting an ellipse to back-projected image rays from a minimum of three views of the experiment. This is possible because it is known that the cross-sections of certain anisotropic materials will change from initially cylindrical to elliptical under applied loading [4], however other deformed cross-sectional shapes that may be sensibly approximated as elliptical could be measured using this technique.

In-situ measurements of diametrical strain in elliptically deforming specimens have been made in the past [4] using single-location contacting techniques, but this technique cannot be applied at high strain rates and relies on prior knowledge of the elliptical orientation. Previous work on more general cross-sectional reconstruction has often concentrated on computing arbitrary contours [5] into generalised 3D surfaces. Tubular cross-section measurements can be achieved using a single camera by rotating the specimen [6] or the camera [7] to acquire many views for reconstruction. However, these methods cannot be applied to materials characterisation experiments, where tensile loads of many kN would prevent rotation of the specimen and, at least at high strain rates where acquisition is required on μs time scales, rotation of the camera is impossible.

In the method outlined here, at least three views of a deforming specimen are used to find tangent fan rays from its silhouette. An algorithm that can incorporate any number of tangential rays, is used to find the least-squares fit of an arbitrary ellipse to these fan rays.

The method has been evaluated using simulations of the experimental procedure with stochastic error estimations and by measuring similarly sized elliptical objects that have been accurately measured using a contacting technique. The technique has been applied to tensile dog bone specimens of a commercially available rolled Ti64 alloy that have been loaded quasi-statically and at a high strain rate as a proof of concept.

2. Method

2.1. Image Capture and Processing

The process of obtaining 2D specimen surface coordinates from experiments has three stages: capturing images throughout the experiment, image rectification using predetermined calibration factors and edge detection to identify the specimen outline. These outlines give target lines from the camera centres to the specimen, which are taken forward into the contour reconstruction process.

In both the quasi-static (QS) and high strain rate (HR) experiments presented here cylindrical dog bone tensile specimens with a gauge diameter of 3 mm and a gauge length of 8 mm were used, as seen in figures 3 and 4.

In the QS experiments, three TELI Digital Cameras (CSB4000CL) with 4 megapixel 10-bit greyscale CMOS sensors, using Computar Megapixel lenses, were used to capture three views of a specimen from angles at $-45°$, $0°$ and $45°$, figure 1. One end of the specimen was displaced at 5.6×10^{-6} ms^{-1}, which corresponds to a plastic strain rate of 7×10^{-4} s^{-1}; frames were recorded simultaneously on all cameras at a rate of one every three seconds. The resolution of the images was 6.5 μm/pixel.

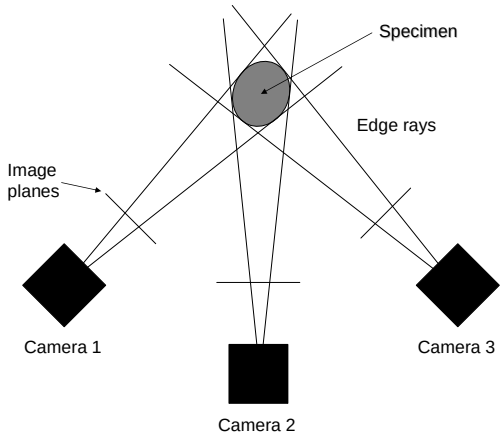

Figure 1. The arrangement of the apparatus for multiple cameras as used in the QS experiments. The angular spacing of 45° between the cameras is a limitation of the equipment and is shown later to be sub-optimal for elliptical fitting.

For HR experiments, a Specialised Imaging SIM16 camera was used with two

mirrors to give views at $-120°$, $0°$ and $120°$, figure 2. HR experiments were performed at a strain rate of $3 \times 10^3 s^{-1}$ in the plastic region; 16 images were recorded at a frame rate of 76 000 frames per second. The resolution of the images was 13 μm/pixel. Strain rates in both QS and HR are quoted ±10%.

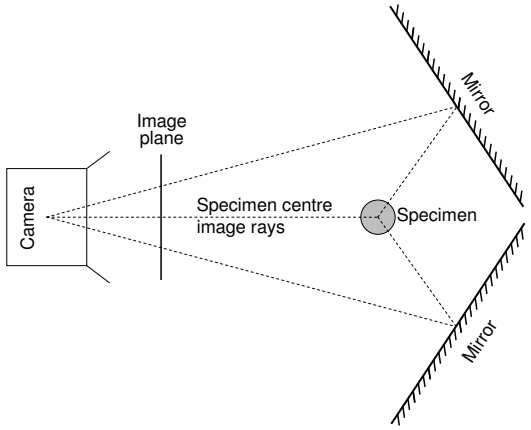

Figure 2. Schematic diagram of the arrangement of the apparatus for single cameras as used in HR experiments. Three views spaced at 120° give well conditioned data for ellipse fitting.

In the QS experiments, the specimen was reverse lit to give a silhouette view for two cameras and front lit for the centre camera, to allow good contrast of the edges in all images. In HR experiments, the specimen's edges are front lit in all views, as shown in figures 3 and 4.

Figure 3. An example of the images captured in one time step in the QS experiments.

The cameras were calibrated using the Matlab Calibration Toolbox [8] to remove intrinsic distortions from the measurements. Extrinsic calibration was performed by measuring the angles between cameras and mirrors to determine camera positions and by using a true cylinder as a reference. Intrinsic and extrinsic calibration are discussed in [9]. The camera lenses were assumed to be telecentric, in that the cameras were assumed to be infinitely far from the specimen, to simplify the extrinsic calibration. The error due to this assumption is explored in Appendix A and found to be negligible.

The edges of the specimen are predominantly vertical. A sub-pixel edge detection algorithm using a 1-dimensional maximum gradient detector was used to determine the positions of the two edges in each view for each pixel row, as shown in figures 5 and 6, with an error of less than ±0.7 μm. These positions give back projections, through the

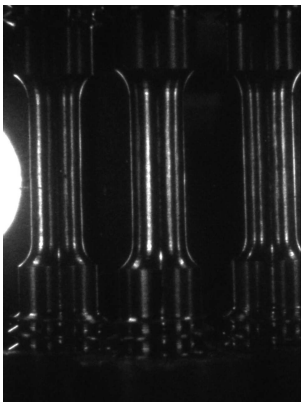

Figure 4. An example of an image captured in one time step in the HR experiments.

camera image planes, which are tangential to the specimen, as shown in figure 1, and will be called tangent lines. At each distinguishable axial position, the back-projected rays may be assumed to lie on a horizontal plane, given the telecentric assumption. The tangent lines are used to reconstruct the elliptical shape of the specimen as a function of axial position and time.

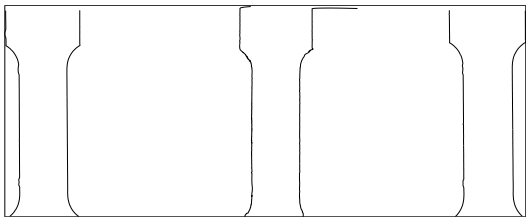

Figure 5. The edges of the QS specimen seen in figure 3.

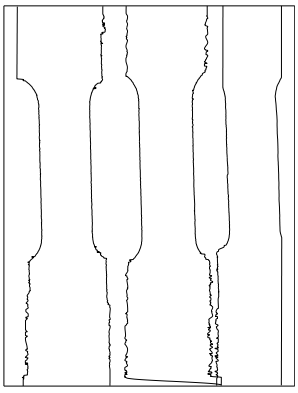

Figure 6. The edges of the HR specimen seen in figure 4.

2.2. Elliptical fitting

The derivation of the conic equation for an ellipse written in the space of the line gradients m and their y-axis intercepts c is as follows:

The back-projected image rays, projected onto a horizontal plane, become, with an appropriate choice of coordinate system orientation, six lines in a plane, two from each camera, of the form:

$$y = m_i x + c_i \quad i = 1, \ldots, 6. \tag{1}$$

If the intersection of the specimen's vertical axis with the horizontal plane is taken to be the origin of the coordinate system, the ellipse never passes through the origin and the elliptical conic section can be represented as an implicit second order polynomial:

$$f = Ax^2 + Bxy + Cy^2 + Dx + Ey + 1 = 0. \tag{2}$$

At the points of tangency (X_i, Y_i), where the lines meet the ellipse, the gradients of the lines and the ellipse have equal directions,

$$\nabla f_i = \begin{bmatrix} 2AX_i + BY_i + D \\ BX_i + 2CY_i + E \end{bmatrix} = \lambda \begin{bmatrix} m_i \\ -1 \end{bmatrix} \tag{3}$$

where λ is an arbitrary scalar. Combining (1), (2) and (3) gives the ellipse defined by any 5 of the 6 lines:

$$f_i = f(m_i, c_i) = A\mu^2 + B\mu\left(m_i\mu + c_i\right) + C\left(m_i\mu + c_i\right)^2 + D\mu + E\left(m_i\mu + c_i\right) + 1 = 0, \tag{4}$$

where:

$$\mu = \frac{-(Bc_i + 2Cm_ic_i + Em_i + D)}{2(A + Bm_i + Cm_i^2)}.$$

Newton's method can be employed to find the parameters, A, B, C, D, E, if only five tangent lines are known. However when six or more lines are known, the elliptical shape is over specified and a least squares solution may instead be used to find the closest fit. In the experiments presented here a Gauss Newton procedure was used to minimise $\sum_i {f_i}^2$ to find the least squares solution.

The Gauss Newton procedure requires an initial estimate for the conic parameters $\boldsymbol{a} = [A, B, C, D, E]^T$ which, for all time steps but the first, may be taken as conic shape in the previous step at the same axial position because the shape change between frames is small. The estimates for the first time step are taken to be circles. These circles are centred at the centroid of triangle formed by the (three, for these experiments) lines bisecting each camera's pair of back-projected rays. The circle's radius is taken as the mean distance from this centre to all of the rays.

3. Estimation of error

Elliptical prisms of precisely known dimensions were measured using the technique described above to estimate the accuracy in practice using the specified equipment. Also, the experiment has been simulated to estimate the optimum values of certain parameters to obtain data of the highest accuracy and to obtain a generic estimate of the accuracy likely to be achieved.

3.1. Static reconstruction of elliptical prisms

Prisms with prescribed elliptical shapes were wire eroded to provide reference cross-sectional geometry. Four prisms were produced with nominal minor and major axes lengths of 3.464×3.464 mm, 3×4 mm, 2.5×4.8 m and 2×6 mm. The prisms were measured using a Mitutoyo SERIES 191 CNC Controlled Coordinate Measurement Machine, with an accuracy of better than ± 2 μm for each of approximately 200 points measured around the circumference. Reconstructions of these prisms using the QS equipment are shown in figure 7 and the errors in the measurements are shown in figure 8.

In experiments on the titanium alloy, ellipticities, $e = a/b$, of no more than 0.18 were observed, which should have an accuracy of better than the $\pm 5\%$ error encountered for the prism of $e = 1.33$.

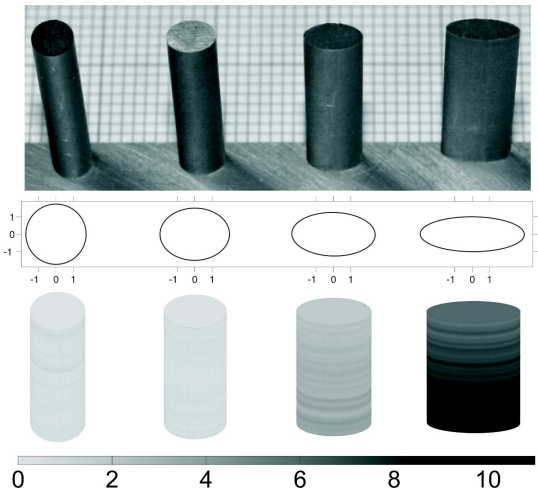

Figure 7. The elliptical prisms, their measured cross-sectional shape and reconstructions shaded according to the percentage error in a/b.

3.2. Statistical simulations of the fitting

The effect of varying camera positions and specimen shape was investigated using a stochastic method. The experimental variables simulated can be seen in figure 9. For a particular ellipse, each tangent line was perturbed perpendicularly by a normally distributed random value to mimic the errors encountered during real experiments. The perturbed lines were used to fit ellipses using the method described. This process was repeated 1000 times for each set of simulation parameters. The simulated noise was chosen to be normally distributed with mean $\mu = 0$‡ and standard deviation $\sigma = 0.01$ to represent the accumulated error from all possible sources, including lens calibration, extrinsic calibration and lighting changes, amongst others. The percentage

‡ These values are dimensionless as they represent ellipses with an area of π, and all lengths are normalised to give a mean radius of 1.

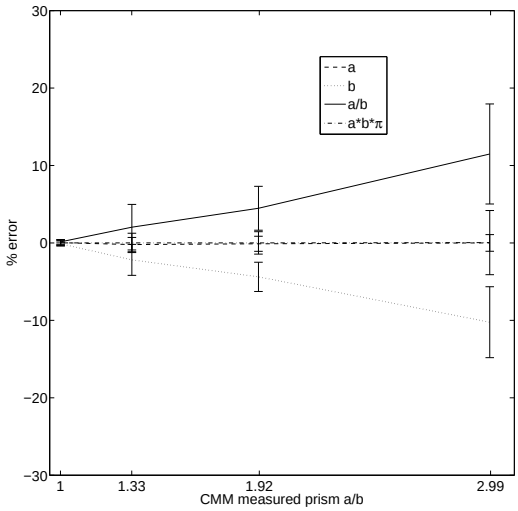

Figure 8. Actual reconstruction of elliptical prisms.

errors, E_i, were calculated using the resultant value from each of the 1000 simulated reconstructions, x_i, and the true value, $\hat{x}$, to give $E_i = 100(x_i - \hat{x})/\hat{x}$, $i = 1, 2, \ldots, 1000$, for each variable. The means, μ, and error bars $\pm 2\sigma$ of these values are shown in figure 10 for a simulation where L = 1000, $\phi = 90°$, $\theta = 45°$ and ellipse area = π, the values of ϕ and θ match those used in the reconstruction of elliptical prisms discussed in 3.1.

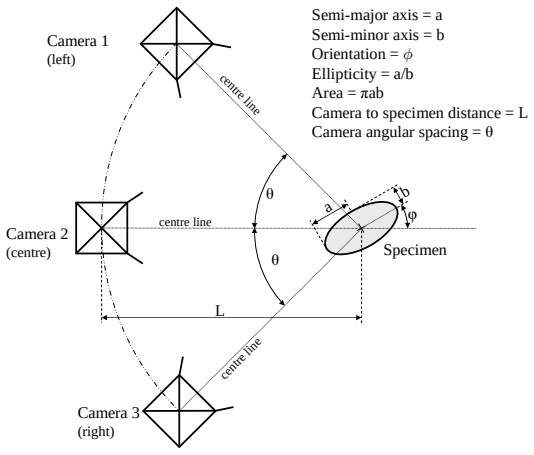

Figure 9. The simulated experimental variables

It will be shown later that $\phi = 90°$ and $\theta = 45°$ are the most poorly conditioned combination of orientation and spacing so the results in 3.1 represent a worst case. Comparison of figures 10 and 11 show that cameras equally spaced at 60° (or equivalently 120°) from one another, are typically of the order of 10 times more accurate than cameras placed at 45° for large ellipticities.

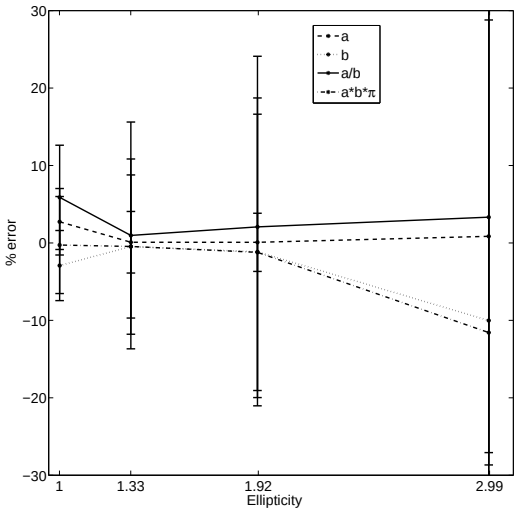

Figure 10. Simulated reconstruction of ellipses for cameras angularly spaced at 45°.

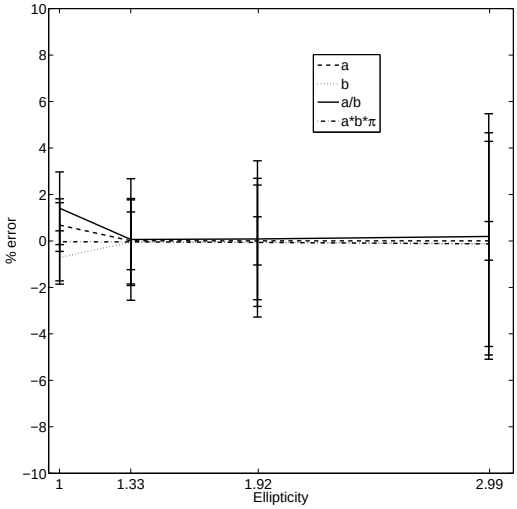

Figure 11. Simulated reconstruction of ellipses for cameras angularly spaced at 60°. The scale has been altered from figure 10 for clarity.

Figure 12 shows a comparison of error as a function of ϕ for $\theta = 45°$ and $\theta = 60°$. It was observed that $\phi = 90°$ and $\theta = 45°$ gives the greatest errors, as it gives rise to poorly conditioned data for the least squares fitting with large ellipticities. Much of the data is concentrated around two points on the ellipse, figure 13, and as a result, the value of b is poorly conditioned whilst a is well determined.

The poor result at $e = 1$ in the simulations, figures 10 and 11, compared to the reconstruction of the real prisms in 3.1 is because the simulations are biased so that any deviation from circular at $e = 1$, whether positive or negative, will increase the positive error because e is defined to be positive for all shapes. Whereas, in the experiments, cylindrical specimens are used as part of the extrinsic calibration procedure and will

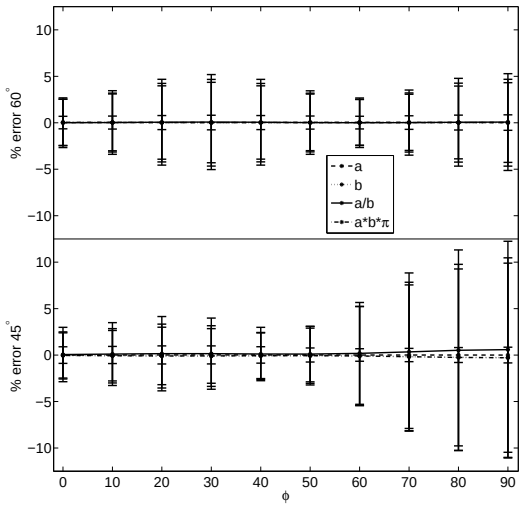

Figure 12. An ellipse with $e = 3$ has been simulated in the 45° and 60° camera arrangements for a range of orientations, ϕ. The trends in the error bars demonstrate that the most accurate determination of elliptical shape is when cameras are pointed along the ellipse's major and minor axes directions. It can be seen that the 45° cameras have particularly poor errors at $\phi = 90°$, because the data is poorly conditioned, as demonstrated in figure 13. These simulations were run with a factor of 10 lower variance than for figures 10 and 11 to allow for an easier comparison between the angles of ϕ. Other orientations outside of these ranges of ϕ are symmetric and need not be shown here.

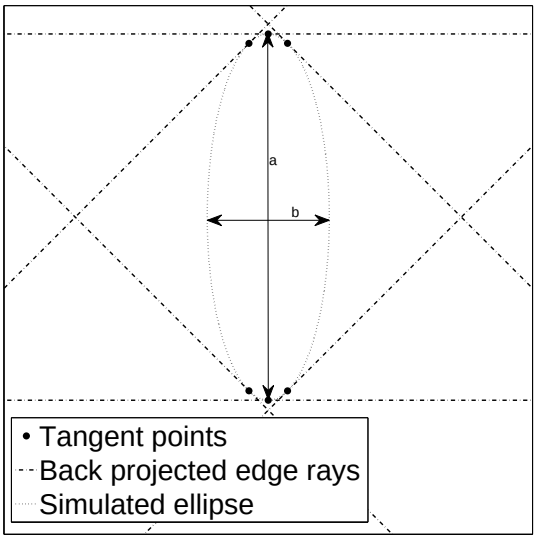

Figure 13. A simulation of an ellipse that gives rise to poorly conditioned data because the camera orientations and the ellipse's orientation cause the points of tangency to group around the extremities. Thus, the value of a is well conditioned, whilst the value of b is likely to be inaccurate.

therefore always produce an accurate mean value. It would seem apparent from these simulations that they are not totally representative of the errors encountered during the experiment. The current hypothesis for this discrepancy is that the model of the error - normally distributed random values - is not wholly correct, and some other estimate that takes into account possible systematic errors due to shadows and calibration problems may be required to alleviate this difference. However, the simulations do provide valuable, generic, insight into the optimum experimental set-up.

4. Mechanically loaded specimen reconstruction

Cylindrical tensile dog-bone specimens of a rolled Ti64 alloy were manufactured with their axes aligned with the material's principal rolling direction. The specimens were loaded quasi-statically and at high strain rate, with images acquired as described above. Figures 14 and 15 show full reconstructions of these specimens in the final frame before fracture. The specimens for which experimental results are presented were orientated to give the best conditioned data. As well as the reconstructed shape, stress and ellipticity are shown as functions of position. It should be observed that the specimens form an elliptical cross-section that is most elliptical in the region of greatest plastic strain. The reconstructions demonstrate the capabilities of this method and the data obtainable through its use.

In order to examine stress distribution as a function of time, graphs such as those in figures 16 and 17 are used. Here, the true direct stress is calculated using the measured force on the specimen and the reconstructed cross-sectional area. In the QS experiment, figure 16, the stress generally increases monotonically as a function of time, until necking is observed. The same trend is observed in HR loading; however there are fewer photographs of the event. In both cases the peak stress in the frame before failure is indicated. It is interesting to note the elastic only (no shape change) unloading of the end of the parallel section after the UTS, as expected, compare figures 16 and 20.

From the peak stress in each frame, a true-stress-time curve can be produced, figures 18 and 19. These curves are essentially continuous for QS loading, where many images are available, but less so at HR, as shown. However, comparison with traditional HR data analysis will allow the user to relate this discrete true stress data to more continuous nominal stress measurements. Further, the technique allows ellipticity to be calculated as a function of time and position, figures 20 and 21. A later paper will show how these data can be used to inform material models.

5. Conclusions

An optical technique for estimating cross-sectional shape by measuring planar surface contours of elliptical specimens has been presented. The technique has been shown to work in both quasi-static and high strain rate experiments to quantify anisotropic

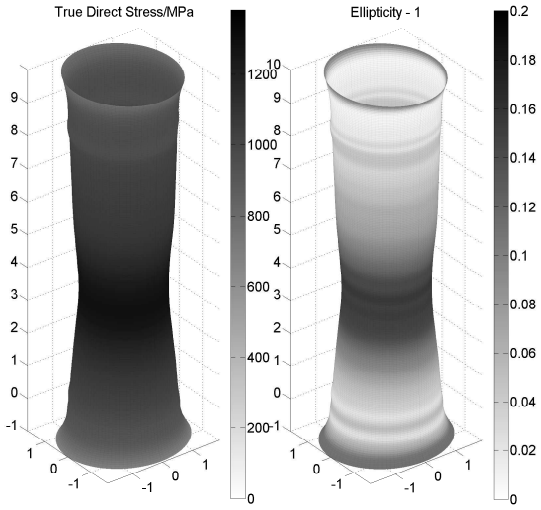

Figure 14. Quasi-static tension specimen at the last recorded time step before fracture.

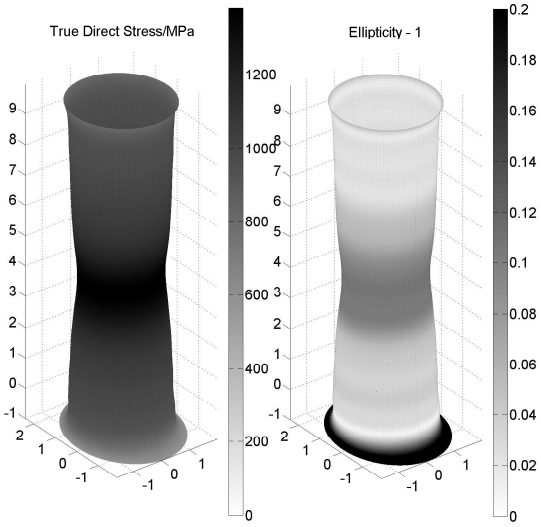

Figure 15. High strain rate tension specimen, at the last recorded time step before fracture.

plasticity behaviour of a titanium alloy for which useful quantitative stress and ellipticity data have been produced.

The technique has been evaluated using computational simulations of the physical conditions that may be encountered in experiments. Stochastic error estimates have been obtained by perturbing the data to mimic the likely deviations of measurements from the true positions. These have shown that the optimal angular spacing of the minimum of three views is 60° or 120°.

Elliptical prisms of precisely known dimensions were reconstructed using the technique, to evaluate both the equipment and the method. It was found that elliptical contours could be measured accurately when orientations and views did not combine to

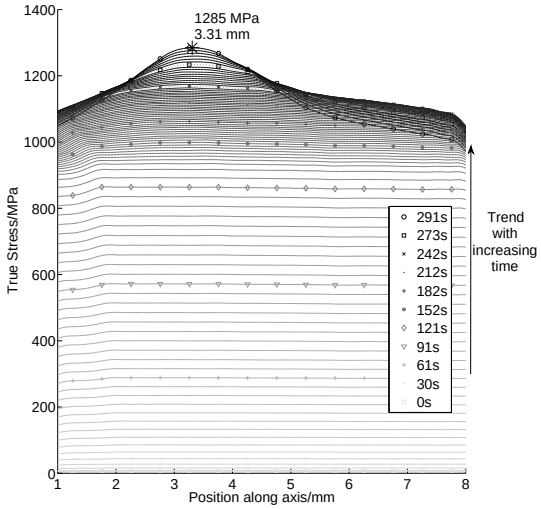

Figure 16. A specimen of cross-rolled Ti64 cut with its axis lying in the plane of rolling. The plots show true direct stress with axial position for several time steps.

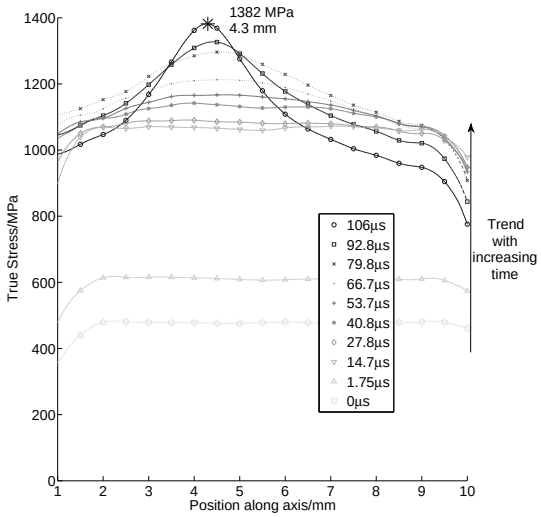

Figure 17. High strain rate direct true stress results

produce poorly conditioned data.

This technique allows the measurement of cross-sectional area, and subsequently total volume, of specimens of anisotropic, homogeneous materials in experiments where three or more views of a cylindrical specimen can be obtained. The technique is applicable in tension or compression tests without the need for contact with the specimen or marking its surface. The technique is well suited to environmentally controlled and high strain rate experiments and may be applied to the measurement of any planar conic section and is not limited to the field of mechanical materials testing.

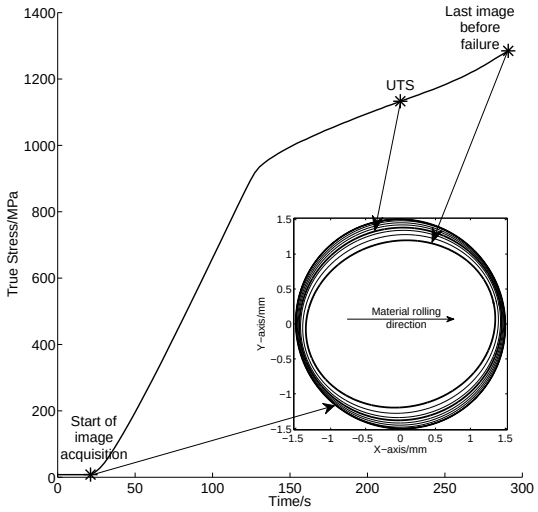

Figure 18. Quasi static true direct stress with time. The inset plot shows the shape of the minimum area cross section at a few selected time steps.

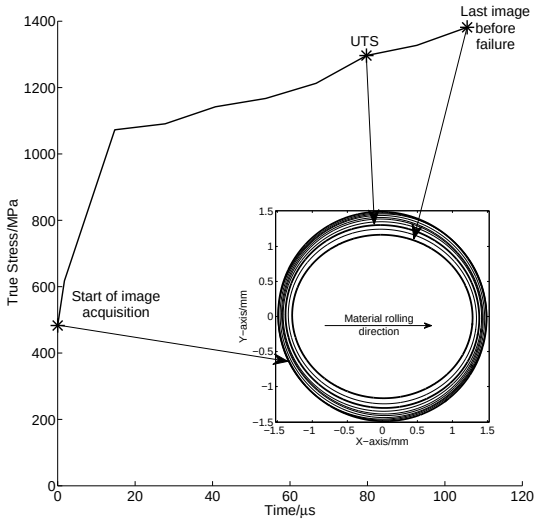

Figure 19. High strain rate true direct stress with time. The inset plot shows the shape of the minimum area cross section at all recorded time steps. Image acquisition was deliberately started after the start of loading so that the limited available frames could be concentrated on plastic deformation.

6. Acknowledgements

This work was supported by the Engineering and Physical Sciences Research Council (EPSRC) and Rolls-Royce plc. The authors acknowledge the colleagues at University of Oxford for their help during the experiments. The SIM16 high speed camera used in this research was provided by the EPSRC instrument loan pool. The authors are particularly grateful to A. Walker for his advice and support whilst using this camera.

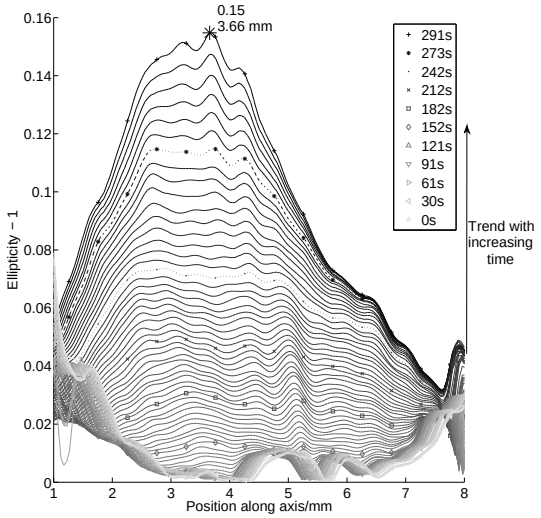

Figure 20. Specimen 1 showing the ratio $a/b - 1$ with axial position and time.

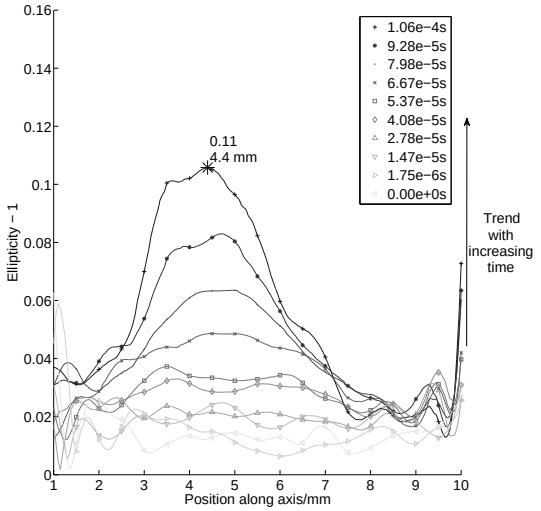

Figure 21. High strain rate ellipticity results

Appendix

Appendix A. Evaluating the Telecentric Assumption

To simplify extrinsic calibration of cameras, an assumption can be made that the cameras are infinitely far from the specimen. This means that light rays are treated as parallel and the back-projected edge rays for elliptical fitting are parallel to the direction in which the camera is pointing. This assumption has been validated and the errors have been quantified by running simulations of the experiment, figure A1. In these simulations the true ellipse tangents to 'near' cameras were calculated. The edge positions of these tangents in images were assumed to lie at the same distance from the camera as the specimen's centre. The image edge positions were used as positions

through which to project parallel rays and these rays provide tangents for fitting a reconstructed elliptical shape.

The normalised distance between the camera and the specimen centre, L, figure 9, was varied with differing values of ellipticity and orientation. An example of the results for the orientation $\phi = 90°$ is shown in figure A2. It was found that for all orientations, camera spacings and ellipticities < 3 the error in the cross-sectional area measured was $< 0.04\%$ for cameras spaced at $L \geq 100$ specimen radii from the specimen centre. For the same range of parameters, the error in ellipticity measured (which was always≤ 0 by definition), for the worst case orientations, was $> -0.017\%$. The error in measuring the orientation of the ellipses was negligible for $L = 100$. In the experiments in this work, no camera was closer than 105 specimen radii to the specimen.

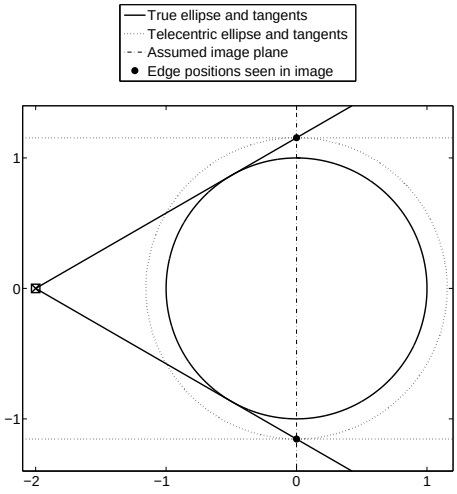

Figure A1. A circular cross-section as seen by one pinhole camera and the true tangential rays through the image edge positions. When the image plane is assumed to lie at the specimen centre and the back-projected rays are assumed to be telecentric, the cross-sectional reconstructed shape is larger than the original. As the camera centre is moved away from the specimen, the error due to the telecentric assumption decreases.

References

[1] Todd M Osman. *ASM Handbook*, volume 8, page 3:12. American Society for Metals, 12 edition, 2000.

[2] Holger Aretz, Odd Sture Hopperstad, and Odd-Geir Lademo. Yield function calibration for orthotropic sheet metals based on uniaxial and plane strain tensile tests. *Journal of Materials Processing Technology*, 186(1-3):221–235, May 2007.

[3] C G'Sell. Video-controlled tensile testing of polymers and metals beyond the necking point. *Journal of materials science*, 27(18):5031–, 1992.

[4] HS Yang, XS Su, and B Bai. Analysis of diametral strain in uniaxial tensile and compression testing of round specimens of anisotropic materials. *International journal of mechanical sciences*, 42(12):2395–, 2000.

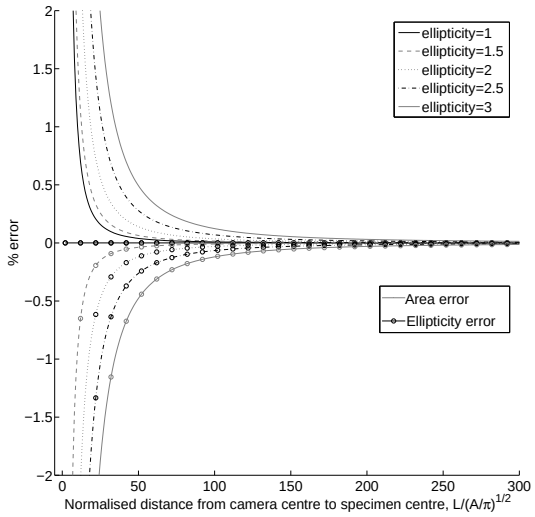

Figure A2. Plots of the percentage error predicted when assuming parallel (telecentric) light rays for an orientation, $\phi = 90°$. The positive plots are the error in the area measurement, which is over-predicted for all ellipticities. The negative plots are for the same simulated fits, but they show the error in the ellipticity (ratio of major to minor axes length) measurement, which is under-predicted for all ellipticities but circular.

[5] P. D. Alevizos, J. Boissonnat, and M. Yvinec. An optimal o(n log n) algorithm for contour reconstruction from rays. In *SCG '87: Proceedings of the third annual symposium on Computational geometry*, pages 162–170, New York, NY, USA, 1987. ACM.

[6] Katia Genovese and Carmine Pappalettere. Whole 3d shape reconstruction of vascular segments under pressure via fringe projection techniques. *Optics and Lasers in Engineering*, 44(12):1311–1323, December 2006.

[7] G T Gullberg, B M W Tsui, C R Crawford, and E R Edgerton. Estimation of geometrical parameters for fan beam tomography. *Physics in Medicine and Biology*, 32(12):1581–1594, 1987.

[8] Jean-Yves Bouguet. Camera calibration toolbox for matlab. *http://www.vision.caltech.edu/bouguetj/calib_doc/ accessed on 09/01/2009.*

[9] R. I. Hartley and A. Zisserman. *Multiple View Geometry in Computer Vision.* Cambridge University Press, ISBN: 0521540518, second edition, 2004.